Vacuum 85 (2011) 898–903

Contents lists available at ScienceDirect

Vacuum

journal homepage: www.elsevier.com/locate/vacuum

Analysis on elastic–plastic spherical contact and its deformation regimes, the one parameter regime and two parameter regime, by finite element simulation

Weimin Chen [a,*], Min Li [b], Yang-Tse Cheng [c]

[a] Lab. of Environmental Mechanics, Institute of Mechanics, CAS, Beijing 100190, China
[b] School of Aeronautics Sciences and Technology, Beijing University of Aeronautics and Astronautics, Beijing 100191, China
[c] Dep. of Chemical and Materials Engineering, University of Kentucky, KY 40506-0046, USA

ARTICLE INFO

Article history:
Received 16 September 2010
Received in revised form
15 December 2010
Accepted 12 January 2011

Keywords:
Contact mechanics
Finite element simulation
Indentation
Contact geometry

ABSTRACT

In this paper the contact problem of a rigid sphere against an elastic–plastic sphere and a spherical elastic–plastic cavity is studied by means of finite element simulation for a wide range of radius ratios. Our results indicate that the deformation range naturally divides into two regimes, i.e. a one parameter regime (covering the elastic, small elastic–plastic and similarity deformation) and a two parameter regime (covering the finite deformation). In these two regimes average contact pressures (as well as contact area) versus indentation depth can be described respectively by the single parameter, i.e. indentation depth h/R_e, and the two parameters, i.e. h/R_e and radius ratio R_1/R_2. Moreover, the variation trends of average contact pressure with the increase of indentation depth differ markedly in different deformation regimes. The numerical evolution of pressure distribution indicates that with increase of indentation depth the pressure distribution becomes more peaked at the center of the contact area meanwhile the maximum contact pressure, limited by the flow stress, increases slightly. Therefore in the two parameter regime, the average pressure would stop growing and get lower rather than continuously higher as it does in the one parameter regime.

1. Introduction

Contact between deformable bodies is a fundamental problem in solid mechanics. And contact problems between spheres have applications in diverse practical problems related to material and surface sciences fields such as tribology, indentation, compaction of granular materials, powder composites, thermal and electrical contacts. For example, instrumented nano-indentations such as spherical indentation have provided valuable information on the mechanical property of materials in very small size in bulk or as thin films and coatings. The insightful understanding of variation of hardness (average pressure) during all indentation process and the influence of contact geometric factors (tip roundness and specimen surface roughness) on hardness behavior are important for obtaining correct mechanical property of materials. For other examples, the cold pressing of metallic powders into a near net shape parts is by the plastic indentation of deformable particles, and predictions of the compaction behavior are based on the knowledge of the location indentation response between particles. The powder composites, such as carbide particle mixed with aluminium alloy powder, have been regarded as a promising material. There is a need to develop accurate prediction models of compaction in order to optimize tooling design and to eliminate manufacturing defects. Therefore, study on the evolution of contact pressure/area and the influence parameter provides a base for resolutions of these material and surface sciences problems.

The problem of elastic contact between two spheres was first solved by Hertz (summarized by Johnson [1]). His work was seminal and initiated a series of studies on problems associated with elastic contact and led to many interesting new solutions [2–4]. Later development extends the work to contact problems between elastic–plastic and visco-elastic–plastic bodies [5–11]. More recently numerical methods have been applied to solve contact problems between spheres for finite deformation [12–14].

The contact deformation can be characterized by the relative displacement h of the centers of the spheres. In the context of indentation this displacement is also known as the depth of indentation. For a fixed h the deformation can be resolved into two distinct components. The first part is a rigid body displacement of one sphere relative to the other, Fig. 1. The second part consists of deformation of the two spheres such that the surface displacements $\overline{u}_1$ and $\overline{u}_2$ meet to form the contact surface. The projection of this surface in the

* Corresponding author. Tel.: +86 010 82543891; fax: +86 010 82338527.
E-mail address: wmchen@imech.ac.cn (W. Chen).

0042-207X/$ – see front matter © 2011 Elsevier Ltd. All rights reserved.
doi:10.1016/j.vacuum.2011.01.007

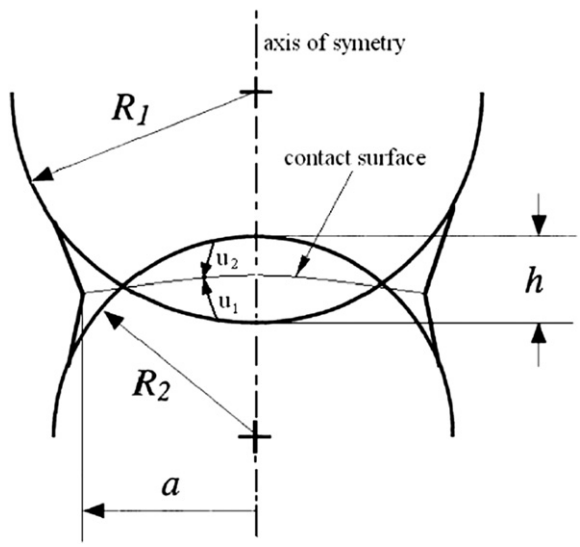

Fig. 1. Geometry of contact between two spheres.

direction of the symmetry axis is the projected contact area. The radius of this area will be denoted by a.

Hertz made the important observation that when h/R_1 and h/R_2 are sufficiently small $\bar{u}_1$ and $\bar{u}_2$ become parallel to the symmetry axis so that these two vectors can be approximated by axial displacements $u_1(r)$ and $u_2(r)$ for $r \le a$. Obviously at $a = 0$, $u_1(0) + u_2(0) = h$. For the same approximation the spherical surfaces can be replaced by equivalent paraboloidal surfaces so that

$$u_1(r) + u_2(r) = h - \frac{r^2}{2}\left(\frac{1}{R_1} + \frac{1}{R_2}\right) \quad \text{for } r \le a \tag{1}$$

Hence Hertz concludes that for sufficiently small h/R_1 and h/R_2 the contact problem can be reduced to two semi infinite space problems subjected to surface compressive stress $\sigma_z(r)$ for $r \le a$ and zero surface stress elsewhere. In the case of elastic contact both the surface stress $\sigma_z(r)$ and radius of the projected area a can be found by solving elasticity problems of the half infinite space subjected to the constraint provided by Eq. (1). This was the way the Hertz solution was obtained.

As radii of the spheres appear only in the combination $(1/R_1) + (1/R_2)$ in the formulation of the contact problem, it can be replaced by a single parameter $(1/R_e) = (1/R_1) + (1/R_2)$. R_e is known as the effective radius [1,15]. Since the Hertz assumption is essentially a geometrical one his method is applicable even when the spheres are not elastic.

Hill et al. [16,17] and Storaker et al. [18] developed similarity solution for the visco-plastic contact between two spheres for power law materials. Like Hertz theory it is also a small deformation theory so that a single parameter R_e representation suffices. Mesarovic and Fleck [19] examined the small deformation (including the elastic, elastic–plastic and similarity solution deformation) and the finite deformation of spherical indentation. From their numerical results (Figs. 4 and 5 of Ref. [19]) it can be observed that with the increase of indentation depth (from small deformation to the finite deformation) the contact pressure behaves differently for different values of radius ratios, though only three special values of radius ratios, i.e. $R_1/R_2 = \infty$, 1, 0 were considered there.

In this paper spherical contact problem is examined for a broader range of R_1 and R_2, i.e. a sphere indenting an elastic–plastic sphere or spherical cavity. And both the small and finite deformation regimes are considered. Section 2 gives the general remarks of spherical contact based on dimensional analysis. Section 3 presents the finite element model and its verification. In Section 4, the numerical results including the evolutions of contact pressure (as well as the contact area) are presented and used to observe the deformation regimes and to explore the variation mechanism of contact pressure especially in the two parameter regime. Conclusions are given in the final section.

2. General remarks

In the general case the elastic–plastic property of each indenter material can be characterized by the Young's modulus E_α, Poison ratio υ_α, the yield stress Y_α and hardening index n_α. Hence the contact force P and radius of the contact area a can be expressed as

$$\frac{P}{E_2 R_1^2} = f_p\left(\frac{h}{R_1}, \frac{R_2}{R_1}, \frac{Y_2}{E_2}, \frac{E_1}{E_2}, \frac{Y_1}{Y_2}, \upsilon_1, \upsilon_2, n_1, n_2\right) \tag{2}$$

$$\frac{a}{R_1} = f_a\left(\frac{h}{R_1}, \frac{R_2}{R_1}, \frac{Y_2}{E_2}, \frac{E_1}{E_2}, \frac{Y_1}{Y_2}, \upsilon_1, \upsilon_2, n_1, n_2\right) \tag{3}$$

or

$$\frac{A}{2hR_1} = \frac{\pi a^2}{2hR_1} = f\left(\frac{h}{R_1}, \frac{R_2}{R_1}, \frac{Y_2}{E_2}, \frac{E_1}{E_2}, \frac{Y_1}{Y_2}, \upsilon_1, \upsilon_2, n_1, n_2\right) \tag{3'}$$

In the case of small deformation characterized by sufficiently small h/R_1 and h/R_2 we can invoke the Hertz assumption and write

$$\frac{P}{E_2 R_e^2} = f\left(\frac{h}{R_e}, \frac{Y_2}{E_2}, \frac{E_1}{E_2}, \frac{Y_1}{Y_2}, \upsilon_1, \upsilon_2, n_1, n_2\right) \tag{4}$$

$$\frac{a}{R_e} = f\left(\frac{h}{R_e}, \frac{Y_2}{E_2}, \frac{E_1}{E_2}, \frac{Y_1}{Y_2}, \upsilon_1, \upsilon_2, n_1, n_2\right) \tag{5}$$

or

$$\frac{\pi a^2}{2hR_e} = f\left(\frac{h}{R_e}, \frac{Y_2}{E_2}, \frac{E_1}{E_2}, \frac{Y_1}{Y_2}, \upsilon_1, \upsilon_2, n_1, n_2\right) \tag{5'}$$

In the case of two spheres $R_e \le R_1$ and R_2. Hence the conditions $h/R_1 \ll 1$ and $h/R_2 \ll 1$ are implied by the single condition $h/R_e \ll 1$. No such simplification is possible in the case of sphere–spherical cavity contact where radius of the spherical cavity is negative.

3. The finite element model of elastic–plastic spherical contact

The present simulation utilizes the commercial program ABQUAS. There exist three contact situations, namely between two spheres, between a sphere and a spherical cavity and between a sphere and a half space (see Fig. 2). The present simulation will focus on the first two cases, because the third case is a limiting case of them. The finite element models are shown in Fig. 3a and b. Triangular three node elements are used. Finer meshes are employed near the region of contact in order to achieve required accuracy. The radius of the contact area is determined by finding the location of the last activated contact element. As the indentation depth increases, successive surface nodes come into contact so that the contact size increases in discrete steps. So in some loading interval the indentation depth h increases by Δh but the contact radius a remains constant (because the number of contact nodes remains constant). On a plot of average contact pressure versus indentation depth h/R_e, the data points would show up as steps. By checking the finite element results against the Hertz solution it was found that a satisfactory fit is achieved by joining the mid-points of the finite element simulation. These results are shown in Fig. 4.

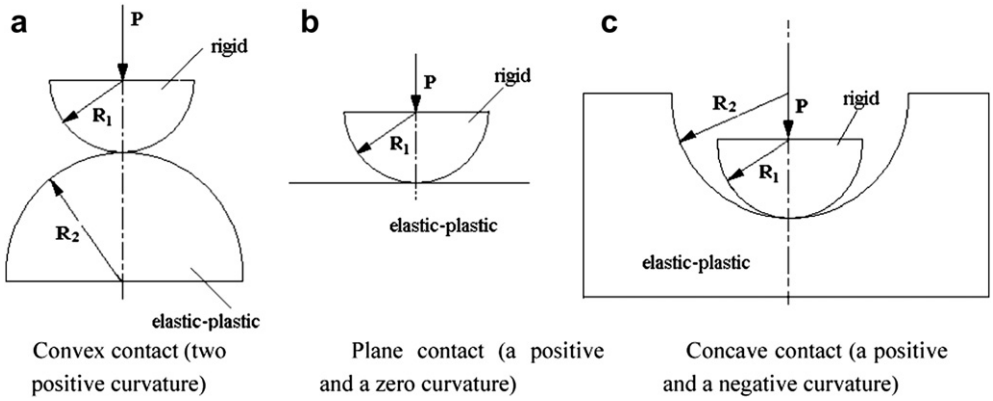

Fig. 2. Three situations of spheres contact.

The radius R_2 of the deformable sphere and cavity is taken to be +50 nm and −50 nm respectively. For the sphere–sphere contact, radius R_1 of the rigid sphere ranges from 10, 20, 40, 62.5, 125, 250 nm. For the sphere–spherical cavity contact R_1 equals to 10, 20, 40 nm. An elastic perfect plastic material is chosen to be our model material. The Young's modulus, Poisson ratio and yield strength are respectively equal to 70 GPa, 0.3 and 200 MPa.

Finite element simulation is carried out for two regimes. For the first regime the deformation is sufficiently small (either $h/R_e \ll 1$ or $h/|R_2| \ll 1$ as the case may be) so that a one parameter representation is valid. This regime covers both elastic and elastic–plastic deformation. The second regime is for large deformation where a two parameter representation is necessary. We call the first regime a single parameter regime and the second a two parameter regime.

4. The numerical results and discussions

Results of finite element simulation for elastic–plastic contact including two regimes are shown in Fig. 5. Fig. 5a is a plot of typical average contact pressure $P/\pi a^2$ versus the non-dimensional penetration depth h/R_e. For clarity only six curves are shown, namely those for radius ratios $R_1/R_2 = 40/(-50)$, $20/(-50)$, $10/(-50)$, 10/50, 40/50 and 250/50. These curves are continuations of the elastic curves shown in Fig. 4. Fig. 5b is a plot of typical non-dimensional contact area $\pi a^2/2hR_e$ against the non-dimensional penetration depth h/R_e.

Fig. 5a demonstrates that at sufficiently small indentation depth (approximately for $h/R_e < 3.0 \times 10^{-3}$) curves with different values of R_1/R_2 almost collapse into a single curve and that the average contact pressure continues to grow with increasing penetration depth h/R_e, though in a way distinct from the Hertz solution (compared with curves in Fig. 4). The former fact confirms the assertion that for sufficiently small values of the indentation depth a single geometric parameter representation (Eq. (3)) suffices no matter what constitutive relation is used and irrespective of whether it is a sphere–-sphere contact or a sphere–spherical cavity contact.

As h/R_e continues to increase the contact enters the two geometric parameter regime and the curves (Fig. 5a) with different values of R_1/R_2 begin to separate and diverge reaching their separate peaks at different depths h/R_e. It is also observed that for the

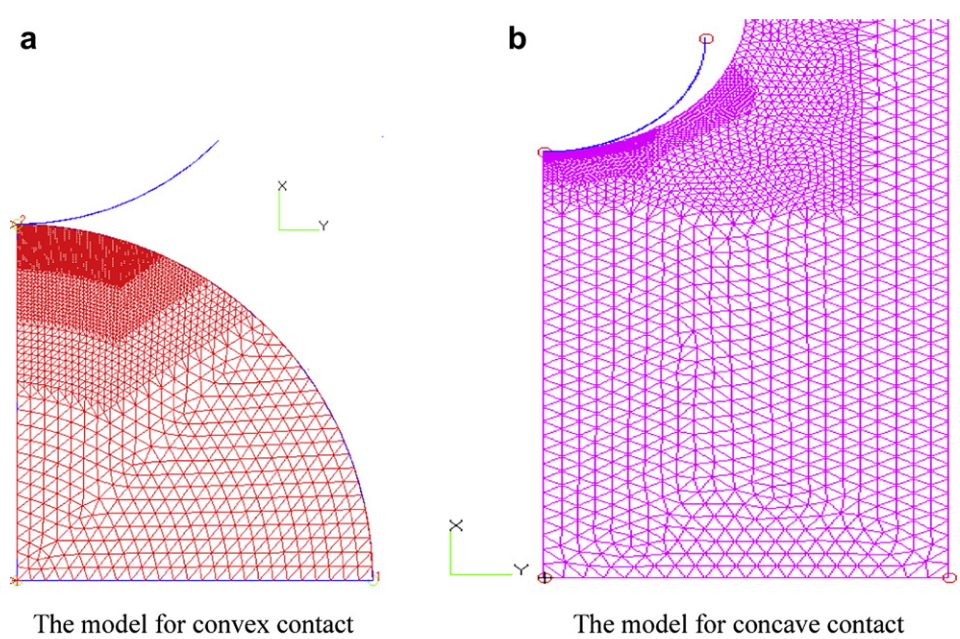

Fig. 3. The finite element model.

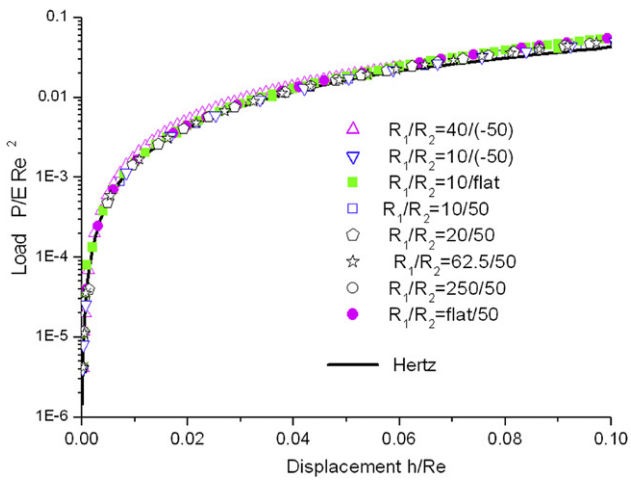

Fig. 4. Finite element simulations for elastic contact.

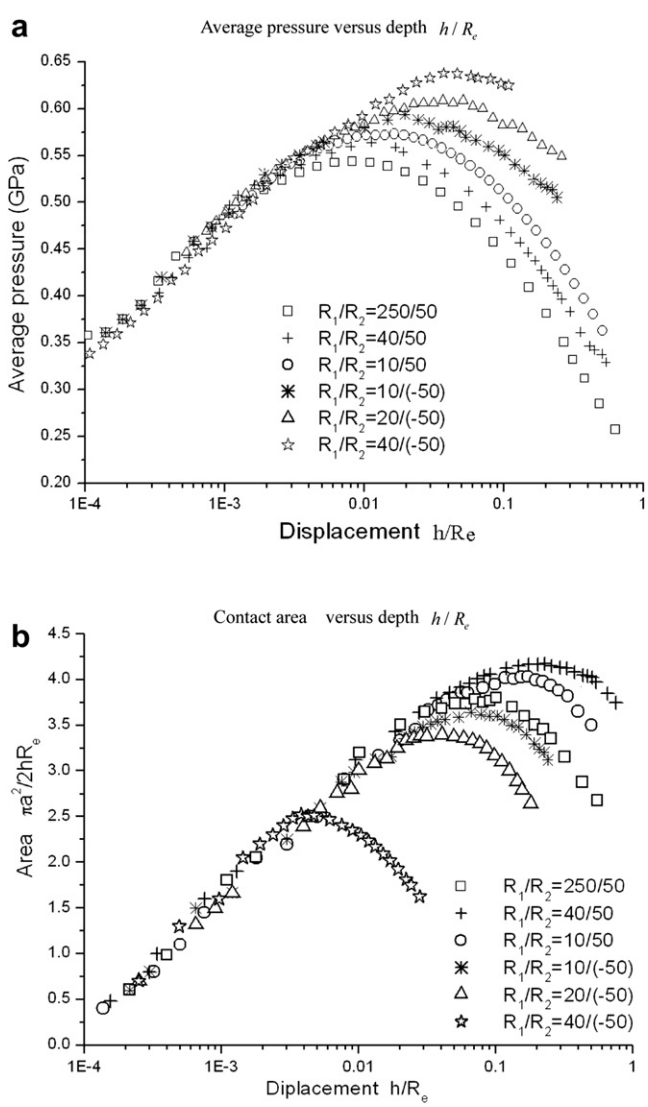

Fig. 5. Finite element simulations for elastic–plastic contact.

sphere–sphere contact, the sharper the relative radius of the indenter is (smaller values of R_1/R_2) the greater the peak average contact pressure is. Additionally, within the two parameter regime, the average pressure diminishes fast with increasing indention depth for large value of R_1/R_2, and slow for small value of R_1/R_2. This was also observed in experiments and other numerical results for two limit cases ($R_1/R_2 = \infty$ and $R_1/R_2 = 0$). The opposite is true in the case of the sphere–spherical cavity contact: the sharper the relative radius (smaller values of $R_1/|R_2|$) the smaller the peak average pressure. Because the larger value of relative radius $R_1/|R_2|$ means the stronger lateral constraint of the indented cavity, the average pressure becomes greater with the increase of relative radius $R_1/|R_2|$.

It is also shown that when the radius of the deformable cavity is equal to that of a deformable sphere while using a same rigid indenter, the average contact pressure is higher in the case of sphere–spherical cavity contact than in the case of sphere–sphere contact (see the curves for $R_1/R_2 = 10/(-50)$ and $R_1/R_2 = 10/50$ in Fig. 5a). This is because in the former case lateral constraint to deformation is stronger. Again from the physical point of view, in the limit of the half space (namely R_1/R_2 or $R_1/|R_2| \to 0$) these two sets of peak values must converge. This requires that the peak average pressure increases as R_1/R_2 decreasing in the case of sphere–sphere contact and decreases as $R_1/|R_2|$ decreasing in the case of sphere–spherical cavity contact, and reaches to the same limit value as the radius ratios approaching zero (R_1/R_2 or $R_1/|R_2| \to 0$).

Contact area $\pi a^2/2hR_e$ plotted against the indentation depth h/R_e in Fig. 5b also demonstrates a one parameter regime for small indentation depth (approximately for $h/R_e < 3.0 \times 10^{-3}$) and a two parameter regime for large indentation depth. Additionally, it is noted that effect of radius ratio R_1/R_2 on the maximum contact area is no longer monotonic. As the values of R_1/R_2 increase from -0.8 ($R_1/R_2 = 40/(-50)$) up to $+50$ ($R_1/R_2 = 250/50$), the maximum contact area first gets larger and then gets smaller.

Fig. 6a shows that the indentation depth, where the peak value ($(P/E_2R_e^2)_{max}$) of the average contact pressure occurs, monotonically becomes smaller with the increase of radius ratio R_1/R_2. Because the smaller values of radius ratio means the sharper indenter for sphere–sphere contact and stronger lateral constraint for sphere–spherical cavity respectively, the average pressure becomes higher. Moreover, for sphere–sphere contact as the indentation depth increases, the influence of free boundary of the deformable body becomes more pronounced, so the average pressure drops. Thus, the drop in the average pressure occurs at a lower value of indentation depth for case of the relative size of the deformable body being smaller, i.e. R_1/R_2 being larger. However the indentation depth, where the peak value ($(\pi a^2/2hR_e)_{max}$) of contact area occurs, first increases till the radius ratio near to 1.0 and then drops with the increase of radius ratio R_1/R_2, as shown in Fig 6b. In other words, a change of behavior is observed around a radius ratio of 1.0 where the radius of the indenting rigid sphere changes from being smaller to larger than the indented sphere. In two parameter regime, for the case of $R_1/R_2 < 1$ (the limit is a rigid sphere indenting into a deformable flat, $R_1/R_2 = 0$), the increase of contact area is mainly provided by more local deformation of material extruded away by the rigid indenter. Thus, the normalized contact area $\pi a^2/2hR_e$ approaches its peak early, i.e. at a lower value of indentation depth, for case of the relative size of the deformable body being larger (R_1/R_2 being smaller) due to stronger boundary constraint. While for the case of $R_1/R_2 > 1$ (the limit is a rigid flat contacting against a deformable sphere, $R_1/R_2 = \infty$), the increase of contact area is mainly provided by more totally pressed deformation of the deformable body. Thus, the normalized contact area $\pi a^2/2hR_e$ approaches its peak easily, or at a lower value of indentation depth, for case of the relative size of the deformable body being smaller,

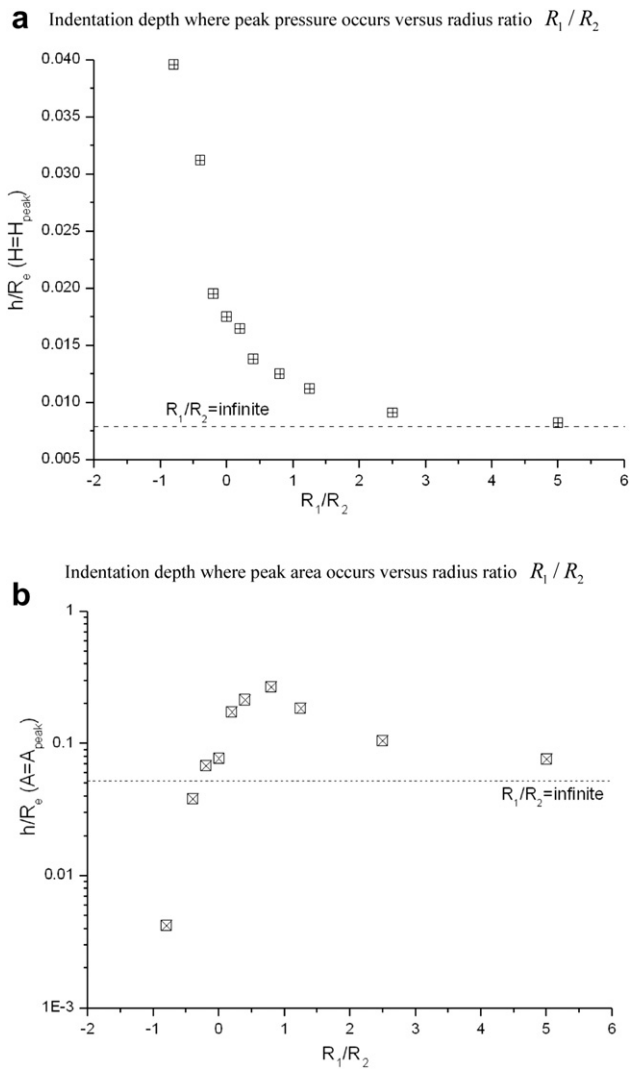

Fig. 6. Indentation depth where peak value of pressure (or area) occurs with radius ratio R_1/R_2 ranging from $R_1/R_2 = 40/(-50)$ to 250/50.

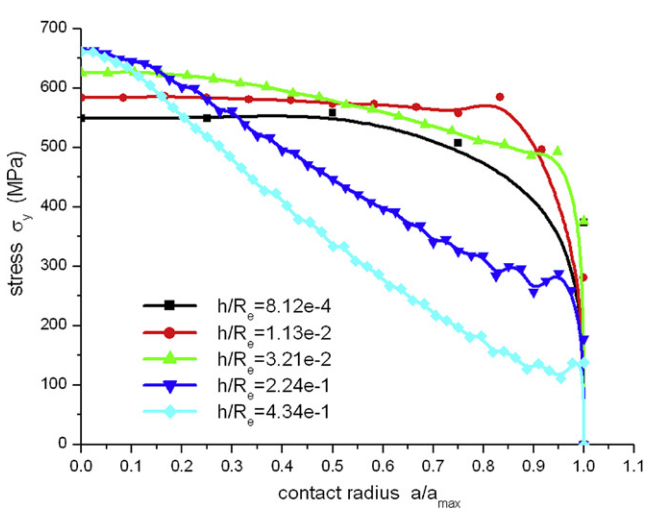

Fig. 7. Pressure distribution at typical indentation depth in the two parameter regime, $R_1/R_2 = 10/50$.

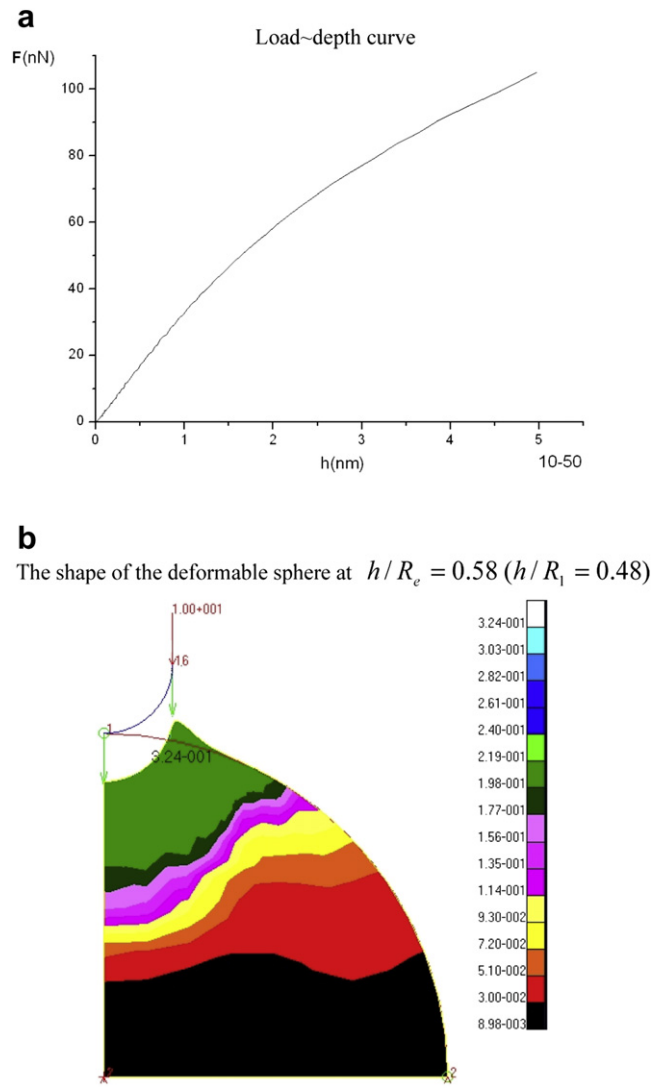

Fig. 8. Results of finite element simulation for $R_1/R_2 = 10/50$.

i.e. R_1/R_2 being larger. Additionally, the pile-up around indentation would be obstructed strongly by larger indenter, so the increase of contact area becomes more difficult for larger value of R_1/R_2.

It is noted in Fig. 5a that in the two geometric parameter regime as the indentation depth increases further, the average contact pressure becomes lower. Fig. 7 presents the evolutions of contact pressure distributions as depth h/R_e increasing from 8.12e−4 to 4.34e−1 for radius $R_1/R_2 = 10/50$. Two interesting phenomena are noted. One is that as the indentation depth increasing the distribution shape of the contact pressure becomes more and more peaked mainly due to drop of stress around the outer edge of contact area. With the increase of indentation depth, the pile-up around the indentation becomes pronounced, which have relatively little stress because of the lack of lateral constraint. Thus there is a significant drop of stress around the area of pile-up (the outer edge of contact area). Another is that the peak value of the contact pressure increases slightly due to the assumption that the examined material is none work hardening. These two evolution phenomena are mainly responsible for the drop of the average contact pressure at large depth. Additionally, Fig. 8a shows the variation of total contact force F against indentation depth for radius $R_1/R_2 = 10/50$ and Fig. 8b shows the shape of the deformed sphere at the maximum depth $h/R_e = 0.58$. It is seen that overall

indentation depth the contact force F increases continuously with the increase of depth h/R_e, as we know normally.

5. Conclusions

By means of finite element simulation the frictionless normal contact of a rigid sphere against an elastic–plastic sphere or a spherical elastic–plastic cavity is examined for a wide range of radius ratios. According to the depth of indentation the deformation naturally divides into two regimes, i.e. the one parameter regime and the two parameter regime. For the cases examined in this paper, further conclusions are as follows:

1. The one parameter regime covers the elastic, the small elastic–plastic and the similarity deformation. In this regime the average contact pressure versus indentation depth is fully described by the single parameter h/R_e, and the pressure increases monotonically with h/R_e. The demarcation of the elastic–plastic regime is marked by the departure from the Hertz solution of elastic contact.
2. As indentation depth continues to increase the single curve describing the average contact pressure versus depth h/R_e begins to branch out in accordance with the values of radius ratio R_1/R_2 so that one enters the two parameter regime where as the depth increasing different branches initially increase until reaching their respective peaks and then begin to drop. This pressure drop is mainly due to the fact that the maximum contact pressure is limited by the flow stress while the distribution of the contact pressure becomes more peaked.
3. Compared with the average contact the contact area $\pi a^2/2hR_e$ against h/R_e behaves in a similar way with one exception, namely the peak value of the contact area is no longer a monotonic function of R_1/R_2.

Acknowledgement

This work was supported by the National Science Foundation of China (10772183) and the Intellectual Innovation Project of the Chinese Academy of Sciences (KJCX2-YW-L07). The authors would like to thank the fruitful discussions with Professor C.M. Cheng in Institute of Mechanics, CAS.

References

[1] Johnson KL. Contact mechanics. 2nd ed. New York: Cambridge University Press; 1985.
[2] Greenwood JA, Williamson JBP. Contact of nominally flat surfaces. Proc R Soc Lond A 1966;295:300–19.
[3] Greenwood JA, Tripp JH. The elastic of rough surfaces. J Appl Mech; 1967 March:153–9.
[4] Francis HA. Application of spherical indentation mechanics to reversible and irreversible contact between rough surfaces. Wear 1977;45:221–69.
[5] Bhushan B. Contact mechanics of rough surface in tribology: single asperity contact. Appl Mech Rev 1996;49(5):275–98.
[6] Vu-Quoc L, Zhang X. An elasto-plastic contact force–displacement model in the normal direction: displacement-driven version. Proc R Soc Lond A 1999;455:4013–44.
[7] Zhao Y, Maletta DM, Chang L. An asperity microcontact model incorporating the transition from elastic deformation to fully plastic flow. ASME J Tribol 2000;122:86–93.
[8] Vu-Quoc L, Zhang X, Lesburg L. A normal force–displacement model for contacting spheres accounting for plastic deformation: force-driven formulation. J Appl Mech 2000;67:363–71.
[9] Ni W, Cheng YT, Cheng CM. An energy-based method for analyzing instrumented spherical indentation experiments. J Mater Res 2004;19:149–57.
[10] Mesarovic SD, Fleck NA. Spherical indentation of elastic–plastic solids. Proc R Soc Lond A 1999;455:2707–28.
[11] Oliver WC, Pharr GM. Measurement of hardness and elastic modulus by instrumented indentation: advances in understanding and refinements to methodology. J Mater Res 2004;19:3–20.
[12] Faulkner A, Arnell RD. The development of a finite element model to simulate the sliding interaction between two, three-dimensional, elastoplastic, hemispherical asperities. Wear 2000;242:114–22.
[13] Kogut L, Etsion I. Elastic–plastic contact analysis of a sphere and a rigid flat. J Appl Mech 2002;69:363–71.
[14] Jackson RL, Green I. A finite element study of elastio-plastic hemispherical contact against a rigid flat. J Tribol 2005;127:343–54.
[15] Bobji MS, Biswas SK. Deconvolution of hardness from data obtained from nanoindentation of rough surfaces. J Mater Res 1999;14(6):2259–68.
[16] Hill R, Storakers B, Zzdunek AB. A theoretical study of the Brinell hardness test. Proc R Soc Lond A 1989;436:301–30.
[17] Hill R. Similarity analysis of creep indentation tests. Proc R Soc Lond A 1992;436:617–30.
[18] Storaker B, Biwa S, Larsson PL. Similarity analysis of inelastic contact. Int J Solids Struct 1997;34(24):3061–83.
[19] Mesarovic SD, Fleck NA. Frictionless indentation of dissimilar elastic-plastic spheres. Int J Solids Struct 2000;37:7071–91.